INTERNATIONAL JOURNAL FOR NUMERICAL METHODS IN ENGINEERING, VOL. 40, 3033–3057 (1997)

VOIGT–REUSS TOPOLOGY OPTIMIZATION FOR STRUCTURES WITH LINEAR ELASTIC MATERIAL BEHAVIOURS

COLBY C. SWAN* AND IKU KOSAKA

Department of Civil and Environmental Engineering, 2128 Engineering Building, The University of Iowa, Iowa City, Iowa 52242, U.S.A.

ABSTRACT

The desired results of variable topology material layout computations are stable and discrete material distributions that optimize the performance of structural systems. To achieve such material layout designs a continuous topology design framework based on hybrid combinations of classical Reuss (compliant) and Voigt (stiff) mixing rules is investigated. To avoid checkerboarding instabilities, the continuous topology optimization formulation is coupled with a novel spatial filtering procedure. The issue of obtaining globally optimal discrete layout designs with the proposed formulation is investigated using a continuation method which gradually transitions from the stiff Voigt formulation to the compliant Reuss formulation. The very good performance of the proposed methods is demonstrated on four structural topology design optimization problems from the literature. © 1997 by John Wiley & Sons, Ltd.

Int. J. Numer. Meth. Engng., **40**, 3033–3057 (1997)

No. of Figures: 13. No. of Tables: 0. No. of References: 38.

KEY WORDS: topology optimization; structural design; concept design; mixing rules; sensitivity analysis

1. INTRODUCTION AND MOTIVATION

Variable topology material layout optimization is much more general than fixed topology shape optimization in that it can lead to spatial material distributions of arbitrary connectedness (or 'topology'). It is performed early in the design of structures or composite material systems to find potentially optimal starting 'concept designs' (Figure 1). Once the gross optimal layout problem is solved, fixed topology shape optimization methods can be employed to fine tune designs. For the sake of both interpretability and manufacturability, designers generally seek discrete or separated material distributions in their final designs. Nevertheless, discrete 'ground structure' truss topology approaches such as those of References 1 and 2 are being increasingly supplemented with continuum or continuous formulations such as those proposed by Kohn and Strang[3] and pioneered by Bendsoe and Kikuchi[4] since they permit more general material layout arrangements. In continuum topology formulations, the material occupying a spatial point $\mathbf{X}$ need not be strictly either material $\mathscr{A}$ or material $\mathscr{B}$ but can instead be some combination or 'mixture' of the two. Various forms of material mixtures are routinely permitted to exist throughout the design domain in intermediate

* Correspondence to: Colby C. Swan, Department of Civil and Environmental Engineering, 2128 Engineering Building, The University of Iowa, Iowa City, Iowa 52242, U.S.A.

CCC 0029–5981/97/163033–25$17.50

Received 12 June 1996
Revised 4 December 1996

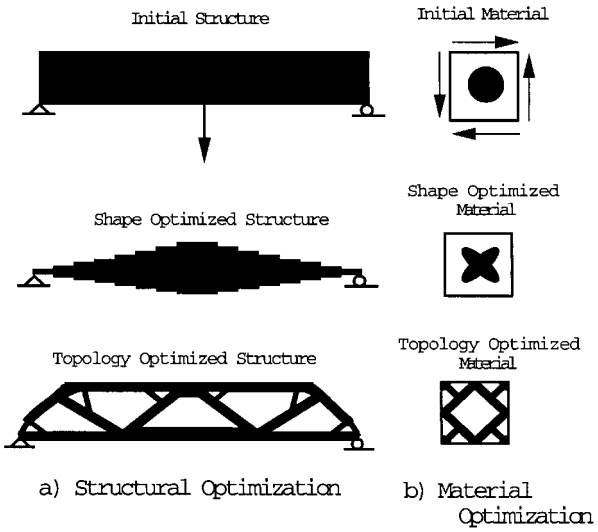

Figure 1. Topology versus pure shape optimization for (a) structures and (b) composite materials. Black regions represent (a) solid material and (b) stiff reinforcing material while white regions indicate (a) void spaces and (b) a compliant matrix phase

and even final design states. By careful formulation and solution of the design problem, however, locally optimal designs can be coaxed to achieve virtually discrete material distributions involving no local mixing.

An important aspect of developing methods to solve continuous, variable topology material layout problems is the constitutive treatment of continuous mixtures of materials. The description, modelling and treatment of such mixtures to obtain their effective mechanical properties as functions of the material phase volume fractions is here denoted by the term 'mixing rules'. Since mixing rules can and do bear a strong influence on the nature of the final solutions obtained, the intent of this paper is to introduce and study the characteristics of a promising new material layout formulation based on classical Voigt and Reuss mixing rules.

Variable topology material layout optimization is presently revolutionizing the design of elastic structures and composite material systems. An open question that remains to be answered is what benefits can be realized by extending these potent layout methods to structures and materials operating in non-linear and inelastic regimes of behavior. Among the numerous obstacles that must be overcome in extending topology design to more general applications are:

(a) generalizing continuous 'mixing rules' to inelastic regimes of material behaviour;
(b) formulating and implementing design sensitivity analysis for non-linear structural topology applications; and
(c) reducing the high computing expense of topology design for non-linear systems.

One reason that the continuous formulation being studied here is attractive to the authors is that it addresses the first obstacle above; that is, due to its generality, it can be used straightforwardly with both linear elastic materials and more general path-dependent non-linear materials. Design sensitivity analysis algorithms for applications involving variable topology material layout design of composite microstructures for high stiffness and strength have been implemented and successfully

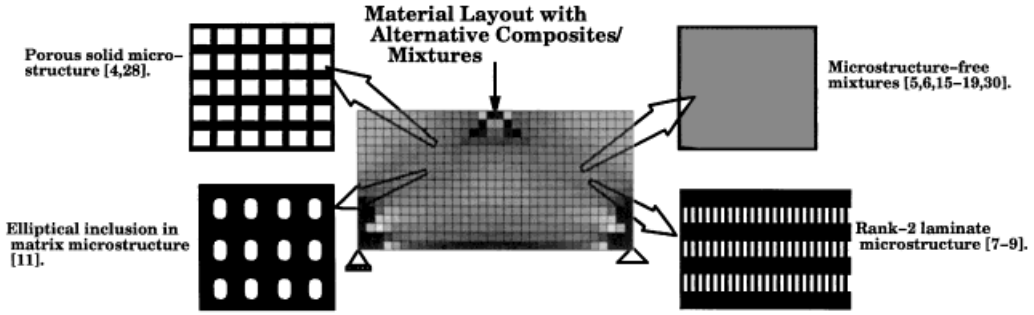

Figure 2. Schematic of variable topology material layout design formulations using alternative classes of composites and/or amorphous mixtures

tested with the proposed formulation in Reference 5. So that the most fundamental characteristics of the new formulation can be studied and established in a controlled environment, however, the scope of this paper is confined to material layout design in linear elastic structures. In a subsequent paper[6] the formulation is extended to deal with general non-linear materials, including the development of non-linear sensitivity analysis for structural systems.

In continuum topology optimization formulations two general classes of methods are presently being employed (Figure 2): (1) relaxed formulations involving assumed parameterized micro-morphologies; and (2) heuristic mixing rules which assume and involve no microstructure. Characteristic of the relaxed formulations utilizing an assumed micro-morphology is the structured porous solid approach proposed by Bendsoe and Kikuchi[4] and widely used in structural topology design to find optimal distributions of solid and void phases. In this method, local mixtures take the form of an assumed periodic porous medium with morphology parameters (a, b, θ) which represent, respectively, the normalized dimensions of the rectangular pores and the pore orientation. Computational homogenization is employed to calculate the effective elastic constants for a discrete sequence of morphology parameters and then in topology optimization numerical interpolation is employed to compute effective elasticity properties of solid–void mixtures for any intermediate values of the morphology parameters.

A conceptually similar method has been used by a number of investigators (for example, References 7–9), who employ structured, rank-2 plane stress laminates in two-dimensions to mix a linear elastic solid phase and a void phase. In the formulation of Jog *et al.*,[7] the laminates are self-adaptive in that their orientation (θ) adjusts to the local strain field to provide a stiff local mixture or 'composite'.[10] One strength of this approach is that for linear elastic and void constituents, analytical formulae rather than computational homogenization is employed to calculate the effective mechanical properties of the mixture. It is recognized, however, that as modelled the self-adaptive laminates are very stiff and do not penalize mixtures of materials in compliance minimization problems as strongly as the homogenization methods do. One consequently ends up with final material layout designs that yield high overall structural stiffness designs by making extensive usage of stiff 'mixtures' or 'composites'.

An alternative relaxed formulation based on an assumed micro-morphology in the material layout is the Mori–Tanaka mixing rule employed by Gea.[11] The Mori–Tanaka mixing rule[12] is based on the physical assumption of dilute suspensions of ellipsoidal particles of material $\mathscr{A}$ embedded in a matrix of material $\mathscr{B}$ and uses analytical Eshelby solutions[13] to predict the elastic properties of

the mixtures based solely on the volume fraction and assumed particle shapes and orientations of the respective phases. This mixing rule can in principle be used in inelastic topology optimization since its usage for inelastic materials is already established as, for example, in the constitutive modelling of elastoplastic particulate composites.[14]

The class of mixing rules which assume no micro-morphology of the mixture have the advantage (when used with isotropic materials) of using only a single scalar volume fraction or density parameter to characterize the two-material mixtures in both two and three dimensions. Most prominent among the mixing rules in this category are the simple density based power laws originally investigated by Bendsoe[15] and now widely used by others.[16–19] While these laws are not believed to have an underlying physical basis, they have been effectively and convincingly employed in topology design applications involving linear elastic solid and void phases. They also appear to be readily usable with general elastic and/or inelastic solids.[6]

The new formulation under study here employs no microstructure of the mixtures and uses hybrid combinations of the classical Reuss[20] and Voigt[21] mixing rules to quantify the effective mechanical properties of general multi-material mixtures as functions of volume fractions. A well-known fact of composite mechanics[22] is that the uniform stress Reuss mixing rule significantly underpredicts the observed strength and stiffness of most mixtures (or composites), and is typically employed only to obtain a very loose lower bound on these properties. It is equally well established that the uniform strain Voigt rule typically provides a loose upper bound on the strength and stiffness of most mixtures. Since the aim of this work is *not* to provide accurate constitutive models of mixtures, but rather to provide a continuous and differentiable algorithmic method for obtaining the stress–strain behaviours of mixtures of general materials in a way that consistently penalizes mixtures, the highly compliant nature of the Reuss mixing rule can in fact prove to be potentially advantageous for many topology design applications. Specifically, since many topology design problems involve designing structures to have high strength and stiffness with economy of material, usage of the highly compliant Reuss rule and compliant Voigt–Reuss hybrids treats mixtures as highly compliant and weak which translates to a very inefficient usage of limited material resources. Topology design formulations based on compliant mixing rules therefore tend to achieve final layout designs that are highly discrete.

Topology design formulations that use highly penalized formulations are, in a sense, continuous generalization of the discrete integer programming approaches investigated by Kohn and Strang[3] and found to be unstable. It is thus not surprising that usage of highly compliant hybrid Voigt–Reuss topology formulations without any stability precautions can result in unstable 'checkerboarding' material layout solutions.* Checkerboarding material layout solutions have also been observed in finite element studies of bone adaptation phenomena.[24, 25] For both topology design and bone adaptation studies, a proved solution to the checkerboarding problem has been to use basis functions for the material distribution parameters that vary much more slowly in space than do those of the displacement fields. Effectively, this can be achieved either by using:

(a) high-order finite element methods matched with low-order material distribution fields[23, 26]; or
(b) low-order finite element methods in combination with filtering and/or spatial convolution methods for the material distribution variables.[17, 27, 28]

* It has recently been shown by Jog and Haber[23] in a study on the instabilities that lead to checkerboarding, that stiff topology formulations (i.e. pure Voigt and/or rank-2 laminate formulations) are also vulnerable to this problem as well

In this work, a variation on the spatial convolution methods is presented and implemented to assure that stable material layout designs are achieved without the necessity of resorting to higher-order finite elements (quadratic, cubic, etc.). When combined with this stabilizing filtering procedure and exercised on numerous test problems, the hybrid Voigt–Reuss formulations are found to yield stable, locally optimal material layout solutions that are both interpretable and manufacturable.

The remainder of this paper is organized as follows. In Section 2 the framework for describing the distribution of material phases (including mixtures) throughout a fixed spatial design domain for topology design optimization is described. Section 3 reviews the pure Reuss and Voigt mixing rules and introduces a family of hybrid combinations of the two. The continuous structural topology design problem for linear elastic structures is then formulated in Section 4 complete with design sensitivity analysis. Section 5 presents a novel volume-averaging design variable filter to achieve stable 'checkerboard-free' designs and a brief discussion on uniqueness of solutions based on convexity. The performance of the proposed new class of mixing rules on linear elastic structural topology design calculations is demonstrated in Section 6 on four challenging test design problems previously published in the literature. The general performance of the proposed formulation is assessed in Section 7 and preliminary conclusions are drawn.

2. DISTRIBUTION OF MATERIALS

In the following development, the complete undeformed spatial domain of the structure being designed is denoted by $\mathbf{\Omega}_B$; its designable subset by $\mathbf{\Omega}_D$; and its non-designable subset in which the spatial/topological arrangement of materials is taken to be fixed by $\mathbf{\Omega}_N$. The arrangement of N pre-selected candidate materials in $\mathbf{\Omega}_D$ remains to be determined and so this region is called *designable*. A set of single or multiple loading/boundary conditions to which $\mathbf{\Omega}_B$ will be subjected are specified and a starting design $\mathbf{b}^{(0)}$ which specifies the initial material layout in the $\mathbf{\Omega}_D$ is selected. For each set of loading/boundary conditions, the structure is analysed as a boundary value problem. (For simplicity, attention is restricted here to quasi-static single loading conditions, although the method can be applied equally well to dynamic and/or multiple loading conditions also.) The objective of the design process is to iteratively improve upon the initial design of the structure (that is the spatial arrangement of the N candidate materials in $\mathbf{\Omega}_D$) until an optimal design is achieved. Accordingly, an objective functional which measures the desired behaviour of the structure must be specified, along with constraint functionals which place restrictions on the design, and side constraints which place explicit bounds on the values that can be taken by the individual design variables.

Since the design of the structure is considered to be the spatial distribution of the N candidate materials throughout the spatially fixed design domain $\mathbf{\Omega}_D$, a system is needed to describe the material distributions. For the discrete two-material layout problem involving material $\mathscr{A}$ and material $\mathscr{B}$, the binary indicator function describing the arrangement of material $\mathscr{A}$ would be

$$\chi_{\mathscr{A}}(\mathbf{X}) = \begin{cases} 1 & \text{if material } \mathscr{A} \text{ fully occupies point } \mathbf{X} \in \mathbf{\Omega}_D \\ 0 & \text{otherwise} \end{cases} \tag{1}$$

while that for material $\mathscr{B}$ would be

$$\chi_{\mathscr{B}}(\mathbf{X}) = \begin{cases} 1 & \text{if material } \mathscr{B} \text{ fully occupies point } \mathbf{X} \in \mathbf{\Omega}_D \\ 0 & \text{otherwise} \end{cases} \tag{2}$$

The respective domains $\Omega_{\mathscr{A}}$ and $\Omega_{\mathscr{B}}$ occupied by materials $\mathscr{A}$ and $\mathscr{B}$ would simply be

$$\Omega_{\mathscr{A}} = \{\mathbf{X} \in \mathbf{\Omega}_{\mathrm{D}} \mid \chi_{\mathscr{A}}(\mathbf{X}) = 1;\ \chi_{\mathscr{B}}(\mathbf{X}) = 0\} \tag{3a}$$

$$\Omega_{\mathscr{B}} = \{\mathbf{X} \in \mathbf{\Omega}_{\mathrm{D}} \mid \chi_{\mathscr{B}}(\mathbf{X}) = 1;\ \chi_{\mathscr{A}}(\mathbf{X}) = 0\} \tag{3b}$$

Preference is given in this work to discrete final material distributions $\Omega_{\mathscr{A}}$ and $\Omega_{\mathscr{B}}$ that satisfy equations (3). Such distributions are achieved, however, using continuous formulations which permit *mixtures* to exist throughout the design domain $\mathbf{\Omega}_{\mathrm{D}}$. By permitting mixtures, the material phases $\mathscr{A}$ and $\mathscr{B}$ are allowed to simultaneously and partially occupy an infinitesimal neighbourhood about each spatial point $\mathbf{X}$ in $\mathbf{\Omega}_{\mathrm{D}}$. In describing the mixtures, the binary indicator functions above are no longer useful, but a straightforward and continuous generalization of the binary indicator function concept is available using the volume fraction concept. As employed here the volume fraction of material phase $\mathscr{A}$ at a fixed spatial point $\mathbf{X}$ in the design domain $\mathbf{\Omega}_{\mathrm{D}}$ is denoted by $\phi_{\mathscr{A}}(\mathbf{X})$ and represents *the fraction of an infinitesimal volume element surrounding point* $\mathbf{X}$ *occupied by material* $\mathscr{A}$. The volume fraction definition for material phase $\mathscr{B}$ and others is similar. Natural constraints upon the spatial volume fractions for the two-material problem are

$$0 \leqslant \phi_{\mathscr{A}}(\mathbf{X}) \leqslant 1; \quad 0 \leqslant \phi_{\mathscr{B}}(\mathbf{X}) \leqslant 1; \quad \phi_{\mathscr{A}}(\mathbf{X}) + \phi_{\mathscr{B}}(\mathbf{X}) = 1 \tag{4}$$

The last physical constraint of (4) states that the material volume fractions at $\mathbf{X}$ are not independent. Thus in two-material problems as treated in this paper, one need only be concerned with the layout of phase $\mathscr{A}$ since that of phase $\mathscr{B}$ follows directly from $(4)_3$. The volume fraction method of describing material distributions neither relies upon nor assumes a microstructure or morphology of the local mixture and is a very straightforward generalization of the binary indicator function approach.

In the proposed topology design optimization framework, the design domain $\mathbf{\Omega}_{\mathrm{D}}$ will be discretized into NEL low-order finite elements such as bilinear continuum degenerated shell elements or trilinear three-dimensional continuum elements. For these low-order elements, the independent material volume fraction $\phi_{\mathscr{A}}$ is taken as piecewise constant over the spatial domain occupied by individual finite elements. The designable spatial/topological distribution of material phase $\mathscr{A}$ in $\mathbf{\Omega}_{\mathrm{D}}$ can thus be described by a vector of design variables $\mathbf{b}$ with contributions from each element comprising $\mathbf{\Omega}_{\mathrm{D}}$. Specifically, the design vector $\mathbf{b}$ has the definition:

$$\mathbf{b} := \{\phi_{\mathscr{A}_1}, \phi_{\mathscr{A}_2}, \ldots, \phi_{\mathscr{A}_{\mathrm{NEL}}}\} \tag{5}$$

That is, the full vector of design variables $\mathbf{b}$ is comprised of NEL scalar-valued element level contributions $\phi_{\mathscr{A}_i}$, each of which represents the volume fraction of phase $\mathscr{A}$ in the ith element. This system allows the two candidate materials to be arbitrarily distributed throughout the NEL finite elements comprising the design domain $\mathbf{\Omega}_{\mathrm{D}}$, subject only to natural constraints such as $\phi_{\mathscr{A}i} + \phi_{\mathscr{B}i} = 1$, and $\phi_{\mathscr{A}i} \in [0, 1]$ for each $i \in \{1, 2, \ldots, \mathrm{NEL}\}$.

Global material cost constraints are generally imposed upon the designed structure by specifying appropriate upper or lower limits on the global volume fraction of the independent material phase. A typical upper bound for a solid phase is represented as $\langle \phi_{\mathscr{A}} \rangle - C_{\mathscr{A}} \leqslant 0$, where $C_{\mathscr{A}}$ is a designer

specified upper bound value on the global volume fraction of material phase $\mathscr{A}$ in the structural domain $\mathbf{\Omega}_B$. The global volume fraction of phase $\mathscr{A}$ over the structural domain is calculated as

$$\langle \phi_{\mathscr{A}} \rangle = \frac{\int_{\mathbf{\Omega}_B} \phi_{\mathscr{A}}(\mathbf{X})\, d\mathbf{\Omega}_B}{\int_{\mathbf{\Omega}_B} d\mathbf{\Omega}_B} \tag{6}$$

3. CONSTITUTIVE MIXING RULES

3.1. Generalized Voigt and Reuss mixing rules

Since each finite element in the model of the design domain $\mathbf{\Omega}_D$ contains two material volume fractions of general elastic or inelastic solids, a critical issue that must be addressed is how these materials are combined at the finite element level, or more basically at the integration point level, to form effective stress–strain relations. Toward this end, the basic properties and characteristics of Voigt, Reuss and hybrid Voigt–Reuss mixing rules are discussed here.

In a strict sense, the physical motivation behind the classical Voigt and Reuss mixing rules has significance only for the very special case of one-dimensional composites or mixtures. For such mixtures, the Voigt rule assumes that the phases are arranged in parallel (Figure 3) so that when loaded axially the strain in each material will be the same. The Reuss rule assumes the phases are arranged in series so that the stress in each will be the same. The one-dimensional Voigt arrangement leads to very stiff, strong mixtures, whereas the Reuss arrangement leads to compliant and weak behaviours (Figure 4).

Whereas the stiffness of the Reuss mixture (Figure 4(a)) smoothly transitions from $E_{\mathscr{B}}$ at $\phi_{\mathscr{A}} = 0$ to $E_{\mathscr{A}}$ at $\phi_{\mathscr{A}} = 1$ the strength behaviour of the Reuss mixture is discontinuous. The nature of the discontinuity arises from the fact that the strength of the Reuss mixture (Figure 4(b)) is controlled by the strength of the weaker constituent $\mathscr{B}$ for $\phi_{\mathscr{A}} < 1$, and by the stronger constituent at $\phi_{\mathscr{A}} = 1$. Since continuity and piecewise differentiability are desired of the mixture behaviours, this feature is unacceptable. To alleviate this problem, and to achieve a more controllable behaviour of the mixture which will be quite useful in all topology optimization applications, both elastic and inelastic, a hybrid Voigt–Reuss mixture such as that shown in Figure 5 is proposed.

For multi-dimensional mixtures, it is generally not possible to devise an equilibrium arrangement of materials that satisfies either the Voigt or Reuss conditions for all potential loading conditions.[22] Nevertheless, the Voigt and Reuss rules can be generalized to higher dimensions simply by assuming that the phases share the same local strain tensor (Voigt) or the same local stress tensor

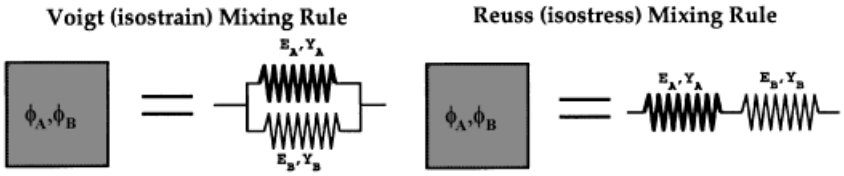

Figure 3. Schematic of Voigt (parallel) and Reuss (series) mixtures. Both materials are characterized by their stiffnesses E and strengths Y

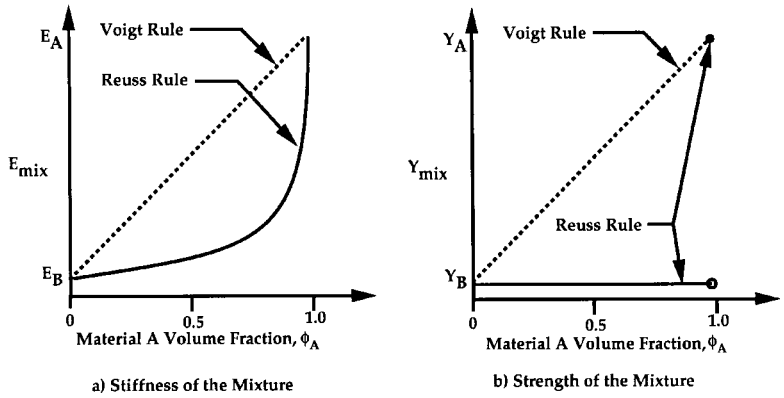

Figure 4. Schematic of effective stiffness E (a) and strengths Y (b) of the two-material Voigt and Reuss mixtures. For the diagrams shown, material $\mathscr{A}$ is taken to be stiffer and stronger than material $\mathscr{B}$

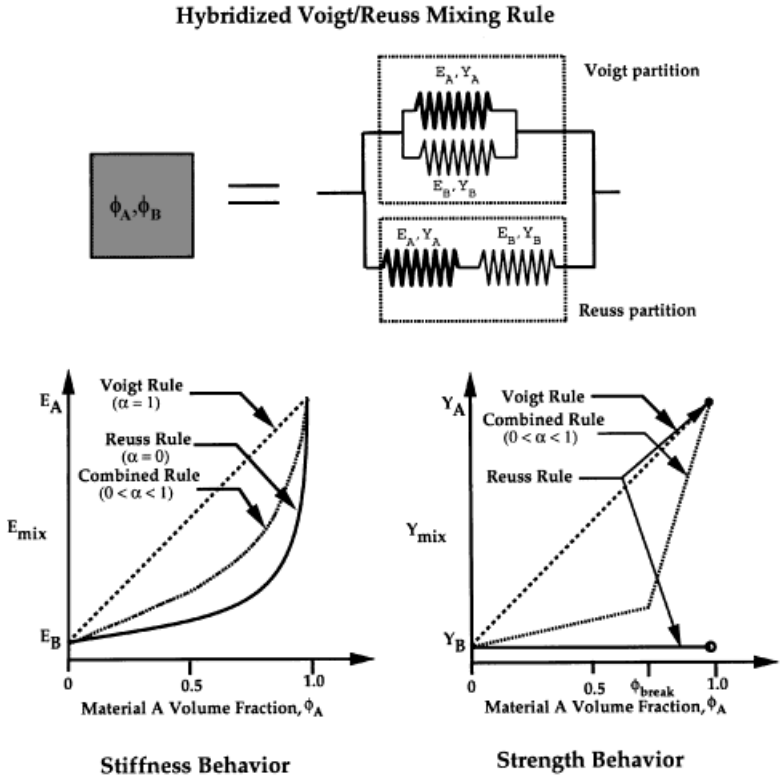

Figure 5. Schematic of effective stiffness (a) and strengths (b) of the hybridized Voigt–Reuss mixture. For the diagrams shown, material $\mathscr{A}$ is taken to be stiffer and stronger than material $\mathscr{B}$

(Reuss) under all possible loading conditions. Accordingly, the decomposition equations for the Voigt mixing of two general phases at a given material point $\mathbf{X}$ are as follows:

$$\boldsymbol{\varepsilon}_{\text{Voigt}} = \boldsymbol{\varepsilon}_{\mathscr{A}} = \boldsymbol{\varepsilon}_{\mathscr{B}} \tag{7a}$$

$$\boldsymbol{\sigma}_{\text{Voigt}} = \phi_{\mathscr{A}} \boldsymbol{\sigma}_{\mathscr{A}}(\boldsymbol{\varepsilon}) + \phi_{\mathscr{B}} \boldsymbol{\sigma}_{\mathscr{B}}(\boldsymbol{\varepsilon}) \tag{7b}$$

The corresponding decomposition equations for the Reuss mixing of two general phases are:

$$\boldsymbol{\varepsilon}_{\text{Reuss}} = \phi_{\mathscr{A}} \boldsymbol{\varepsilon}_{\mathscr{A}} + \phi_{\mathscr{B}} \boldsymbol{\varepsilon}_{\mathscr{B}} \tag{8a}$$

$$\boldsymbol{\sigma}_{\text{Reuss}} = \boldsymbol{\sigma}_{\mathscr{A}}(\boldsymbol{\varepsilon}_{\mathscr{A}}) = \boldsymbol{\sigma}_{\mathscr{B}}(\boldsymbol{\varepsilon}_{\mathscr{B}}) \tag{8b}$$

For the hybrid Voigt–Reuss mixture (Figure 5), the assumption is that both branches of the mixture have the same strain and that the volume fraction of the total mixture in the Voigt branch is α and that in the Reuss branch is $1 - \alpha$. Accordingly, the effective stresses and strains of the partitioned mixture are

$$\boldsymbol{\varepsilon} = \boldsymbol{\varepsilon}_{\text{Voigt}} = \boldsymbol{\varepsilon}_{\text{Reuss}} \tag{9a}$$

$$\boldsymbol{\sigma} = \alpha \boldsymbol{\sigma}_{\text{Voigt}} + (1 - \alpha) \boldsymbol{\sigma}_{\text{Reuss}} \tag{9b}$$

There are numerous options on how one can treat the hybridizing parameter α. Here, it is proposed that α be treated as follows:

$$\alpha = \begin{cases} \alpha_0, & 0 \leqslant \phi_{\mathscr{A}} \leqslant \phi_{\text{break}} \\ \alpha_0 + (1 - \alpha_0) \frac{(\phi_{\mathscr{A}} - \phi_{\text{break}})}{(1 - \phi_{\text{break}})}, & \phi_{\text{break}} < \phi_{\mathscr{A}} \leqslant 1 \end{cases} \tag{10}$$

where $\alpha_0 \in [0, 1]$ and $\phi_{\text{break}} \in (0, \infty)$ are constants chosen to achieve desired mixture behaviours. By choosing α_0 and ϕ_{break} appropriately, one can obtain the Voigt mixing rule, the Reuss mixing rule, or any intermediate combination of the two. For both stiffness and strength characteristics, the hybrid Voigt–Reuss mixing rule is continuous and piecewise differentiable. Strength characteristics of hybrid mixtures are not continuously differentiable at $\phi = \phi_{\text{break}}$. This generally does not pose a problem so long as ϕ_{break} is not selected as either '0' or '1' which are the expected terminal values for volume fraction design variables.

3.2. Special case: linear isotropic solid and Void materials

Application of the Voigt and Reuss mixing rules to the treatment of elastic and inelastic solids has been treated by the authors in Reference 6. Here attention is confined to the special case of mixing a linear isotropic elastic solid phase and a void phase. Young's modulus E and Poisson's ratio v are commonly used material constants to characterize the elasticity tensor of linear isotropic elastic solids. In a mixture of a linear isotropic elastic solid and a void phase, the void phase does not contribute to the stiffness of the mixture. For simplicity, one can therefore choose the Poisson's ratio of the void phase as equal to that of the solid phase, $v_{\text{void}} = v_{\text{solid}}$. Thus, only the effective Young's modulus for the mixture E_{mix} needs to be computed since the Poisson's ratio of the mixture will be equal to that of the solid and void phases, $v_{\text{mix}} = v_{\text{void}} = v_{\text{solid}}$.

In the Voigt mixing rule, usage of isostrain conditions (7) gives an effective Young's modulus of the mixture as

$$E_{\text{Voigt}} = \phi_{\text{solid}} E_{\text{solid}} + \phi_{\text{void}} E_{\text{void}} \tag{11}$$

Similarly, using the Reuss isostress assumption (3.2) gives an effective Young's modulus for the mixture as

$$E_{\text{Reuss}} = \left[\frac{\phi_{\text{solid}}}{E_{\text{solid}}} + \frac{\phi_{\text{void}}}{E_{\text{void}}}\right]^{-1} \tag{12}$$

For mixtures containing both Voigt and Reuss partitions, the effective Young's modulus for the mixture is simply

$$E = \alpha E_{\text{Voigt}} + (1 - \alpha) E_{\text{Reuss}} \tag{13}$$

where α is the volume fraction of the mixture in the Voigt partition (10).

Although the Young's modulus E_{void} of the void phase is theoretically zero, a small stiffness E_{void} compared to that of the solid phase E_{solid} must be maintained to avoid singularity of the finite element equations. In the event that the stiffness of the void phase is chosen too large, the structure will derive some stiffness from the void phase, which is unrealistic. Striking a balance between these two extremes, the stiffness ratio in this paper is taken as $E_{\text{void}}/E_{\text{solid}} = 10^{-6}$ since our numerical experiments show it to provide very good performance and results.

For the special case under consideration, a strength of the Voigt and Reuss mixing rules is that the stiffnesses of mixtures can be written as simple, analytical, and differentiable expressions of the volume fractions ($\phi_{\text{solid}}, \phi_{\text{void}}$). As will be discussed in Section 4 in the context of design sensitivity analysis, the quantity $\partial\sigma/\partial\phi_A|_{\mathbf{u}}$ must be computed. For the special cases under consideration, this quantity is easily computed as

$$\left.\frac{\partial \boldsymbol{\sigma}}{\partial \phi_{\text{solid}}}\right|_{\mathbf{u}} = \frac{\partial \mathbf{C}}{\partial \phi_{\text{solid}}} : \boldsymbol{\varepsilon} \tag{14}$$

To evaluate $\partial\mathbf{C}/\partial\phi_{\text{solid}}$ in (14), one needs only to take the derivative of the effective Young's modulus E with respect to the design variables, i.e.

$$\frac{\partial E_{\text{Voigt}}}{\partial \phi_{\text{solid}}} = E_{\text{solid}} - E_{\text{void}} \tag{15a}$$

$$\frac{\partial E_{\text{Reuss}}}{\partial \phi_{\text{solid}}} = \left[\frac{1}{E_{\text{void}}} - \frac{1}{E_{\text{solid}}}\right] [\phi_{\text{solid}} E_{\text{solid}} + \phi_{\text{void}} E_{\text{void}}]^{-2} \tag{15b}$$

The derivative of E for hybrid mixtures is thus simply

$$\frac{\partial E}{\partial \phi_{\text{solid}}} = \alpha \frac{\partial E_{\text{Voigt}}}{\partial \phi_{\text{solid}}} + (1 - \alpha) \frac{\partial E_{\text{Reuss}}}{\partial \phi_{\text{solid}}} + (E_{\text{Voigt}} - E_{\text{Reuss}}) \frac{\mathrm{d}\alpha}{\mathrm{d}\phi_{\text{solid}}} \tag{16}$$

4. THE TOPOLOGY DESIGN FORMULATION

4.1. Objective and constraint functionals

Numerous formulation options exist in structural topology design optimization in terms of utilizing assorted combinations of objective and constraint functionals. The design variables as specified in (5) are continuous and real-valued; it is assumed that dependent functionals, both objective and constraints, will also be continuous, real-valued, and piecewise differentiable.

It is useful to distinguish between purely cost based functionals which are independent of the response of the system being designed (that is $\mathscr{F} = \mathscr{F}(\mathbf{b})$) and performance based functionals which by definition depend upon both the design variables $\mathbf{b}$ and the performance or state of the designed system which can generally be described in terms of $\mathbf{u}$, the vector displacement field (that is $\mathscr{F} = \mathscr{F}(\mathbf{b}, \mathbf{u})$). An example of a pure cost functional for the structural topology optimization problem is the overall volume fraction of one of the candidate constituent phases, defined as

$$\mathscr{F}_{\phi_{\mathscr{A}}} = \langle \phi_{\mathscr{A}} \rangle - \mathscr{C}_{\mathscr{A}} \tag{17}$$

in which $\langle \phi_{\mathscr{A}} \rangle$ represents the volume average of $\phi_{\mathscr{A}}$ over the entire analysis domain $\mathbf{\Omega}_{\mathrm{B}}$. In contrast, the global strain energy functional over the analysis domain for general loading conditions is a performance functional and would be defined as

$$\mathscr{F}_{\mathrm{E}} = \int_0^t \int_{\mathbf{\Omega}_{\mathrm{B}}} \boldsymbol{\sigma} : \dot{\boldsymbol{\varepsilon}} \, \mathrm{d}\mathbf{\Omega}_{\mathrm{B}} \, \mathrm{d}\tau \tag{18}$$

where τ is a parametric time variable. A typical topology design optimization problem might be to minimize the strain energy functional $\mathscr{F}_{\mathrm{E}}$ of the structure under applied force loadings (thereby maximizing the stiffness of the structure for the applied loads), subject to a volume constraint on phase $\mathscr{A}$. Alternatively, an equally viable way to pose the problem would be to minimize the global volume fraction of material phase $\mathscr{A}$ subject to a constraint on the strain energy functional of the system. Commonly used performance functionals for linear elastic structural problems are the strain energy functional and eigenvalue functionals while examples of pure cost functionals are global volume fraction constraints; perimeter constraints;[29] and intermediate volume fraction penalization functionals,[29] among many others.

The topology design optimization process is iterative in nature, requiring the solution of an analysis problem with each new variation of the design (Figure 6). Intermingled with solving the analysis problem is the evaluation of the objective and constraint functionals as well as their

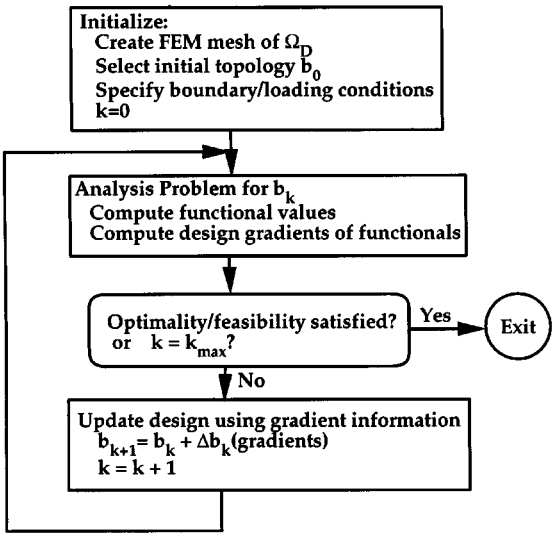

Figure 6. Topology design optimization algorithm

design gradients. The following two subsections formulate the general linear analysis and design sensitivity analysis problems.

4.2. The analysis problem

4.2.1. Linear quasi-static analysis of structures. Topology design can be performed to find the optimal layout of a structure to: minimize compliance; maximize strength; tailor eigenvalues; and tune dynamic response. These varied objectives require the solution of elliptic boundary value problems; eigenvalue problems; and hyperbolic initial and boundary value problems. While the framework under study can and does include all of these classes of problems, attention is restricted here to the class of problems requiring solution of linear static elliptic boundary value problems, the strong form of which is: Find $\mathbf{u}:\boldsymbol{\Omega}_{\mathrm{B}} \mapsto \Re^3$ such that

$$\sigma_{ij,i} + \rho f_j = 0 \quad \text{on } \boldsymbol{\Omega}_{\mathrm{B}} \tag{19}$$

subject to the boundary conditions:

$$u_j(t) = g_j \quad \text{on } \boldsymbol{\Gamma}_{g_j} \text{ for } j = 1,2,3 \tag{20a}$$

$$n_i \sigma_{ij} = h_j \quad \text{on } \boldsymbol{\Gamma}_{h_j} \text{ for } j = 1,2,3 \tag{20b}$$

As is customary, it is assumed that the surface $\boldsymbol{\Gamma}$ of the analysis domain $\boldsymbol{\Omega}_{\mathrm{B}}$ admits the decomposition $\boldsymbol{\Gamma} = \overline{\boldsymbol{\Gamma}_{g_j} \cup \boldsymbol{\Gamma}_{h_j}}$ and $\boldsymbol{\Gamma}_{g_j} \cap \boldsymbol{\Gamma}_{h_j} = \emptyset$, for $j = 1,2,3$. The constitutive behaviour of the material (or mixture of materials) occupying $\boldsymbol{\Omega}_{\mathrm{B}}$ relates the local stress $\boldsymbol{\sigma}$ to local strain $\boldsymbol{\varepsilon} = \frac{1}{2}[(\Delta\mathbf{u}) + (\Delta\mathbf{u})^{\mathrm{T}}]$ through a linear elastic constitutive model of the general form

$$\boldsymbol{\sigma} = \mathbf{C} : \boldsymbol{\varepsilon} \tag{21}$$

The weak or variational form of the problem is obtained by restating the strong form (19) as

$$\int_{\boldsymbol{\Omega}_{\mathrm{B}}} [\sigma_{ij,i}\delta u_j + \rho f_j \delta u_j] \, \mathrm{d}\boldsymbol{\Omega}_{\mathrm{B}} = 0 \tag{22}$$

from which integration by parts, usage of the divergence theorem and utilization of the natural boundary conditions gives the virtual work equation

$$\int_{\boldsymbol{\Omega}_{\mathrm{B}}} \sigma_{ij}\delta\varepsilon_{ij} \, \mathrm{d}\boldsymbol{\Omega}_{\mathrm{B}} = \int_{\boldsymbol{\Omega}_{\mathrm{B}}} \rho f_j \delta u_j \, \mathrm{d}\boldsymbol{\Omega}_{\mathrm{B}} + \int_{\Gamma_h} h_j \delta u_j \, \mathrm{d}\Gamma_h \tag{23}$$

Usage of a Galerkin formulation in which the real and variational kinematic fields are expanded in terms of the same nodal basis functions leads to the following force balance equations at each unrestrained node A in the mesh:

$$\mathbf{r}_{\mathrm{A}} = \mathbf{f}_{\mathrm{A}}^{\mathrm{int}} - \mathbf{f}_{\mathrm{A}}^{\mathrm{ext}} = \mathbf{0} \tag{24}$$

where

$$\mathbf{f}_{\mathrm{A}}^{\mathrm{int}} = \int_{\boldsymbol{\Omega}_{\mathrm{B}}} \mathbf{B}_{\mathrm{A}}^{\mathrm{T}} : \boldsymbol{\sigma} \, \mathrm{d}\boldsymbol{\Omega}_{\mathrm{B}} \tag{25a}$$

$$\mathbf{f}_{\mathrm{A}}^{\mathrm{ext}} = \int_{\boldsymbol{\Omega}_{\mathrm{B}}} \rho N_{\mathrm{A}} \mathbf{f} \, \mathrm{d}\boldsymbol{\Omega}_{\mathrm{B}} + \int_{\Gamma_h} N_{\mathrm{A}} \mathbf{h} \, \mathrm{d}\Gamma_h \tag{25b}$$

For the class of problems being treated here, (24) represents a set of linear algebraic equations which can be solved in any number of ways, a few of which are reviewed in Reference 30.

4.3. Design sensitivity analysis

In any gradient-based (first order) optimization algorithm, it is essential that the total design gradient of the objective and constraint functionals be accurately and efficiently computable. That is, for performance functionals, one must be able to compute

$$\frac{\mathrm{d}\mathscr{F}(\mathbf{b},\mathbf{u})}{\mathrm{d}\mathbf{b}} = \frac{\partial\mathscr{F}}{\partial\mathbf{b}} + \frac{\partial\mathscr{F}}{\partial\mathbf{u}}\frac{\mathrm{d}\mathbf{u}}{\mathrm{d}\mathbf{b}} \tag{26}$$

While the first term in this derivative is easy to compute, the second is somewhat more involved. To evaluate it, the equilibrium state equation for the structure $\mathbf{r}(\mathbf{b},\mathbf{u}(\mathbf{b})) = \mathbf{0}$ (24) must be invoked. Since the equilibrium state equation must be satisfied for all designs, it is true that

$$\mathbf{0} = \frac{\mathrm{d}\mathbf{r}}{\mathrm{d}\mathbf{b}} \tag{27a}$$

$$= \frac{\partial\mathbf{r}}{\partial\mathbf{b}} + \frac{\partial\mathbf{r}}{\partial\mathbf{u}}\frac{\mathrm{d}\mathbf{u}}{\mathrm{d}\mathbf{b}} \tag{27b}$$

$$= \frac{\partial\mathbf{r}}{\partial\mathbf{b}} + \mathbf{K}\frac{\mathrm{d}\mathbf{u}}{\mathrm{d}\mathbf{b}} \tag{27c}$$

Simple rearrangement of (27c) gives

$$\frac{\mathrm{d}\mathbf{u}}{\mathrm{d}\mathbf{b}} = -\mathbf{K}^{-1}\frac{\partial\mathbf{r}}{\partial\mathbf{b}} \tag{28}$$

which can be inserted into (26) to yield

$$\frac{\mathrm{d}\mathscr{F}}{\mathrm{d}\mathbf{b}} = \frac{\partial\mathscr{F}}{\partial\mathbf{b}} - \mathbf{u}^{\mathrm{a}}\cdot\frac{\partial\mathbf{r}}{\partial\mathbf{b}} \tag{29}$$

where $\mathbf{u}^{\mathrm{a}}$, the 'adjoint displacement vector', is the solution of the 'adjoint problem'

$$\mathbf{K}\cdot\mathbf{u}^{\mathrm{a}} = -\frac{\partial\mathscr{F}}{\partial\mathbf{u}} \tag{30}$$

In many topology design optimization problems, the objective is to minimize the compliance (or maximize the stiffness) of a structure to which set of fixed external loads $\mathbf{f}^{\mathrm{ext}}$ are being applied. Minimization of the strain energy or compliance functional (18) associated with a prescribed loading maximizes the stiffness of the structure under the prescribed loading condition. With attention restricted to linear elastic structures, the strain energy functional (18) can be rewritten using conservation of energy in the very simple form:

$$\mathscr{F}_{\mathrm{E}} = \tfrac{1}{2}\mathbf{f}^{\mathrm{ext}}\cdot\mathbf{u} \tag{31}$$

The displacement field that solves the equilibrium condition (24) for linear elastic structures is simply $\mathbf{u} = \mathbf{K}^{-1}\cdot\mathbf{f}^{\mathrm{ext}}$, and the corresponding adjoint displacement vector $\mathbf{u}^{\mathrm{a}}$ that solves the adjoint problem (30) is merely

$$\mathbf{u}^{\mathrm{a}} = -\tfrac{1}{2}\mathbf{K}^{-1}\cdot\mathbf{f}^{\mathrm{ext}} = -\tfrac{1}{2}\mathbf{u} \tag{32}$$

As it was assumed that the external loads $\mathbf{f}^{\text{ext}}$ applied to the structure are independent of the design variables $\mathbf{b}$, the design gradient of the strain energy functional reduces to

$$\frac{\mathrm{d}\mathscr{F}_{\mathrm{E}}}{\mathrm{d}\mathbf{b}} = -\frac{1}{2}\int_{\boldsymbol{\Omega}_{\mathrm{B}}} \boldsymbol{\varepsilon} : \frac{\partial \boldsymbol{\sigma}}{\partial \mathbf{b}}\, \mathrm{d}\boldsymbol{\Omega}_{\mathrm{B}} \tag{33}$$

The quantity $\partial\boldsymbol{\sigma}/\partial\mathbf{b}$ in (33) is here termed the 'stress design gradient', and clearly depends upon the mixing rule being employed. The evaluation of this 'stress design gradient' for both the Voigt and Reuss mixing rules and combinations thereof was treated in Section 3.

5. STABILITY AND UNIQUENESS OF SOLUTIONS

5.1. The checkerboarding problem

In solving material layout problems with penalized Voigt–Reuss formulations, one soon discovers (or rediscovers) that layout designs that are simply discrete are not necessarily desirable, since they might very well contain the studied and documented phenomenon of 'checkerboarding'. To illustrate this point, Figure 7 displays a variety of discrete solutions for the 'three-load bridge problem' (solved previously in References 19 and 31 for example) obtained using the Voigt/Reuss

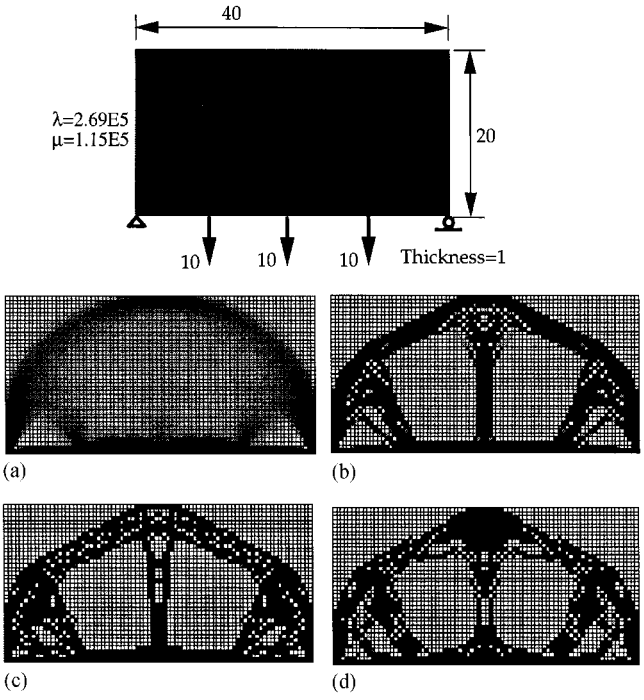

Figure 7. Unstable checkerboarding topology designs and strain energy functional values $\mathscr{F}_{\mathrm{E}}$ for the three-point loaded bridge design problem. The alternative designs were obtained by varying the α parameter described in Section 3. For all designs, $\mathscr{F}_{\phi_{\text{solid}}} = \langle \phi_{\text{solid}} \rangle - 0{\cdot}40 \leqslant 0$: (a) $F_{\mathrm{E}} = 1{\cdot}4123 \times 10^{-2}$, $\alpha = 1{\cdot}0$; (b) $F_{\mathrm{E}} = 1{\cdot}6513 \times 10^{-2}$, $\alpha = 0{\cdot}1$; (c) $F_{\mathrm{E}} = 1{\cdot}735 \times 10^{-2}$, $\alpha = 0{\cdot}01$; (d) $F_{\mathrm{E}} = 1{\cdot}9941 \times 10^{-2}$, $\alpha = 0{\cdot}0$

formulation with varying hybridization parameters α. Most of the solutions show the phenomenon of checkerboarding to some degree. Material layout designs containing this phenomenon are undesirable since:

(a) *They are unstable with mesh refinement*: Checkerboarding solutions are stiff metastable artifacts of finite element and material layout formulations in which the spatial basis functions for displacement fields are not of sufficiently high order in relation to the spatial basis functions for volume fraction design variables. With mesh refinement, checkerboarded layout configurations lose their stability and the layout design must change significantly to regain stability. This cycle can continue indefinitely with increasing mesh refinement, so that convergent material layout solutions that are stable and independent of mesh refinement will not be obtained.
(b) *They are difficult to interpret*: One of the primary reasons for using mixture penalizing formulations is to obtain solutions that are both interpretable and manufacturable. Solutions containing serious checkerboarding are usually neither.

To deal with this problem of unstable, checkerboarding solutions, a simple and mesh-based filtering algorithm is proposed and demonstrated. Perceived benefits of the filter being proposed are that it

(i) is easy to implement;
(ii) permits usage of low-order finite elements;
(iii) works equally well in 2-D, 3-D, and curved shell problems having either regular or irregular meshes;
(iv) does not introduce a new functional into the optimization problem; and
(v) works very effectively.

In continuous two-material layout problems which use low-order bilinear and trilinear finite elements, the volume fractions of the independent material phase are interpolated using basis functions which are uniform over element domains, but generally C^0 discontinuous across element boundaries. For the two-material layout problem, the design vector $\mathbf{b}$ is as defined in (5) and is constituted by the independent material volume fractions in each element. When checkerboarding occurs in layout designs, the discontinuity feature of the design variable basis functions becomes active and volume fractions oscillate rapidly between 0 and 1 across element boundaries in groups of adjacent elements. The problem lies in part with the choice of basis functions for the design variables which permits strong discontinuities across element boundaries.

If one uses spatially low-pass filters on discrete checkerboarding designs $\mathbf{b}$ with a weighted volume-averaging process $\mathscr{H}$ whose averaging domain spans a number of neighbouring elements, then a modified design vector $\mathbf{b}' = \mathscr{H}(\mathbf{b})$ is obtained which contains mixtures and 'grey' zones. The filtered design $\mathbf{b}'$ is smoother, having slower spatial variation and weaker discontinuities across element boundaries than $\mathbf{b}$. If used in conjunction with compliant mixing rules, the filtered representations of checkerboarding designs will behave as compliant grey regions and performance functionals $\mathscr{F}(\mathbf{b}) = \mathscr{F}(\mathbf{b}'(\mathbf{b}))$ will suffer suboptimal performance penalties with checkerboarding solutions. Non-checkerboarding layout designs will thus be obtained by optimization algorithms. If used with spatial filters, the same compliant mixing rules which contribute in part to the checkerboarding problem are therefore a vital aspect of the solution.

Remark 5.1. Previous research efforts[23, 26] have found that checkerboarding instabilities occur when the displacement field basis functions are not of sufficiently high order in relation to those

of the design variable volume fractions. The result of employing low-pass spatial filters on design variables is to *effectively* lower the order of their spatial basis functions relative to those of the displacement field.

5.2. Proposed filter

Among the spatial filtering methods which have been previously investigated to control checkerboarding instabilities are: four-element filters;[28] graphical mesh based filtering methods;[17] and fixed length scale spatial filtering.[17, 27] The latter two methods attempt to eliminate virtually all types of mesh dependencies by introducing fixed length scales on material layout design solutions. The objective of the mesh-based filter proposed here is simply to eliminate checkerboarding in layout designs without necessarily introducing absolute length scales. (If an absolute length scale for the design is desired, then the proposed filter can easily be used in conjunction with a perimeter control method[29] which is an alternative method of imposing fixed length scales on the design.) The filter is applied on an element-by-element basis to all designable elements in the mesh. When applied to say the ith element in a mesh of bilinear elements, the filter produces a modified design variable value b_i' by taking the weighted volume average of the design variables in the ith element and all of its neighbouring elements (Figure 8). In applications that involve bilinear finite elements, only those elements that share nodes with the ith element are considered to be neighbours, with those sharing two nodes classified as first-order neighbours, and those sharing only one node classified as second order neighbours. Using these classifications, the filter is applied to the ith element as follows:

$$b_i' = \frac{b_i V_i + \omega_1 \sum_{j=1}^{n_1^i} b_j V_j + \omega_2 \sum_{k=1}^{n_2^i} b_k V_k}{V_i + \omega_1 \sum_{j=1}^{n_1^i} V_j + \omega_2 \sum_{k=1}^{n_2^i} V_k} \tag{34}$$

where the V's are element volumes; n_1^i is the number of first-order neighbours; and n_2^i is the number of second-order neighbours. The two filtering parameters are $\omega_1 \in [0, 1]$ and $\omega_2 \in [0, 1]$. Typically, the filter is employed with default values $\omega_1 = \frac{1}{2}$ and $\omega_2 = \frac{1}{4}$.

The required modifications to the material layout optimization algorithm when using the proposed filter are minor and easy to implement. With the filter turned on, performance functionals are

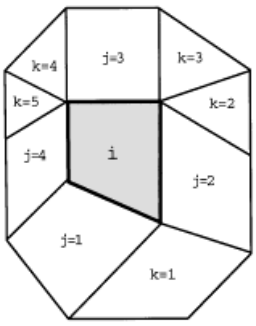

Figure 8. Schematic of a finite element 'i' and its neighbors. First-order neighbours have j indices, while second-order neighbours have k indices

evaluated as $\mathscr{F}(\mathbf{b}) = \mathscr{F}[\mathbf{b}'(\mathbf{b})]$. Accordingly, design gradients are then evaluated using the chain rule as

$$\frac{\mathrm{d}\mathscr{F}(\mathbf{b})}{\mathrm{d}\mathbf{b}} = \frac{\mathrm{d}\mathscr{F}}{\mathrm{d}\mathbf{b}'}\frac{\mathrm{d}\mathbf{b}'}{\mathrm{d}\mathbf{b}} \tag{35}$$

The quantity $\mathrm{d}\mathscr{F}/\mathrm{d}\mathbf{b}'$ is evaluated as discussed in Section 4, and $\mathrm{d}\mathbf{b}'/\mathrm{d}\mathbf{b}$ simply by differentiating (34). High-quality checkerboard-free solutions obtained with the proposed filter are presented in Section 6.

5.3. *Mixing rules and global convexity*

With the proposed filtering methods, stable, checkerboard-free material layout designs can be obtained. In studying the performance behaviour of Voigt and Reuss mixing rules for material layout applications, an additional issue that arises is the uniqueness of solutions obtained for fixed mesh discretizations of the domain $\mathbf{\Omega}_\mathrm{B}$. While not proved, it is assumed that locally optimum solutions $\mathbf{b}^*$ exist such that

$$\mathscr{F}_\mathrm{E}(\mathbf{b}^*) \leqslant \mathscr{F}_\mathrm{E}(\mathbf{b}^* + \delta\mathbf{b}) \tag{36}$$

for all feasible infinitesimal variations $\delta\mathbf{b}$ of the design vector. Our experience in solving numerous linear elastic structural topology problems is that stable local minima satisfying (36) can always be obtained and thus the existence of solutions for a fixed mesh resolution of $\mathbf{\Omega}_\mathrm{B}$ that satisfy (36) does not appear to be an issue.[†] In fact, the problem encountered with highly penalized formulations is that an excessive number of stable local minima satisfying (36) exist for a given meshing of $\mathbf{\Omega}_\mathrm{B}$. Our aim here is to gain some insight into this behaviour with the objective of arriving at the discrete, interpretable, and manufacturable solutions whose performance characteristics approach that of the mathematical global minimum solution $\mathbf{b}_\mathrm{g}^*$ but which is invariably neither discrete, interpretable nor manufacturable.

The issue is briefly studied here using convexity of the strain energy functional [$\mathscr{F}_\mathrm{E} = \frac{1}{2}\mathbf{f}^\mathrm{ext} \cdot \mathbf{u}$] for linear elastic structures subjected to fixed loadings. Insight on the global convexity of $\mathscr{F}_\mathrm{E}$ is related to the definiteness characteristics of its Hessian $\mathrm{d}^2\mathscr{F}_\mathrm{E}/\mathrm{d}\mathbf{b}^2$. An expression for the design gradient of $\mathscr{F}_\mathrm{E}$ for the case of linear elastic structures was derived above as

$$\frac{\mathrm{d}\mathscr{F}_\mathrm{E}}{\mathrm{d}\mathbf{b}} = -\frac{1}{2}\mathbf{u} \cdot \frac{\partial \mathbf{r}}{\partial \mathbf{b}} \tag{37}$$

Taking the derivative of this gradient expression and employing the state equation $\mathbf{r} = \mathbf{0}$ to evaluate $\mathrm{d}\mathbf{u}/\mathrm{d}\mathbf{b}$ gives the Hessian as

$$\frac{\mathrm{d}^2\mathscr{F}_\mathrm{E}}{\mathrm{d}\mathbf{b}^2} = \left(\frac{\partial \mathbf{r}}{\partial \mathbf{b}}\right)^\mathrm{T} \mathbf{K}^{-1} \left(\frac{\partial \mathbf{r}}{\partial \mathbf{b}}\right) - \frac{1}{2}\mathbf{u}^\mathrm{T}\frac{\partial^2 \mathbf{K}}{\partial \mathbf{b}^2}\mathbf{u} \tag{38}$$

In circumstances where the Hessian can be shown to be uniformly positive definite over the entire space of design variables $\mathbf{b}$ and state variables $\mathbf{u}$, solutions to the topology design optimization

[†] Here, attention is restricted to the nature of solutions for fixed mesh resolutions of $\mathbf{\Omega}_\mathrm{B}$. To address the broader issue of the existence of mesh-independent solutions, fixed length scales are imposed on designs either through perimeter control methods[29] or fixed length scale spatial filters[17]

problem which minimizes $\mathscr{F}_{\mathrm{E}}$ will necessarily be unique. In cases where the Hessian is not necessarily positive definite, the functional $\mathscr{F}_{\mathrm{E}}$ will not necessarily be convex, and numerous local optimal might exist.

The first term in (38) is uniformly positive definite for linear elastic materials due to the positive definiteness of $\mathbf{K}$ and its inverse $\mathbf{K}^{-1}$, irrespective of whether the Voigt or Reuss rule is employed. Accordingly, the second term in (38) whose expansion is given below becomes all important in determining the positive definiteness of the Hessian:

$$-\frac{1}{2}\mathbf{u}^{\mathrm{T}}\frac{\partial^2\mathbf{K}}{\partial\mathbf{b}^2}\mathbf{u} = -\frac{1}{2}\int_{\Omega}\boldsymbol{\varepsilon}:\frac{\partial^2\mathbf{C}}{\partial\mathbf{b}^2}:\boldsymbol{\varepsilon}\,\mathrm{d}\Omega \tag{39}$$

Clearly, the character of this term depends upon the mixing rule through the expression $\partial^2\mathbf{C}/\partial\mathbf{b}^2$. Since the stiffness of the Voigt mixture is linear with respect to the design variables [that is $\mathbf{C}_{\mathrm{V}} = \phi_{\mathscr{A}}\mathbf{C}_{\mathscr{A}} + (1-\phi_{\mathscr{A}})\mathbf{C}_{\mathscr{B}}$], the second derivative $\mathrm{d}^2\mathbf{C}_{\mathrm{V}}/\mathrm{d}\mathbf{b}^2$ vanishes. Thus with the Voigt mixing rule, the Hessian of $\mathscr{F}_{\mathrm{E}}$ is globally positive-definite, assuring convexity of $\mathscr{F}_{\mathrm{E}}$ and hence uniqueness of optimization solutions. If one employs the Reuss mixing rule, however, then $\mathbf{C}$ in (39) takes the form

$$\mathbf{C}_{\mathrm{R}} = [\phi_{\mathscr{A}}\mathbf{C}_{\mathscr{A}}^{-1} + (1-\phi_{\mathscr{A}})\mathbf{C}_{\mathscr{B}}^{-1}]^{-1} \tag{40}$$

Differentiating this expression twice yields

$$\frac{\mathrm{d}^2\mathbf{C}_{\mathrm{R}}}{\mathrm{d}\mathbf{b}^2} = 2\mathbf{C}_{\mathrm{R}}\frac{\mathrm{d}\mathbf{C}^{-1}}{\mathrm{d}\phi_{\mathscr{A}}}\mathbf{C}_{\mathrm{R}}\frac{\mathrm{d}\mathbf{C}^{-1}}{\mathrm{d}\phi_{\mathscr{A}}}\mathbf{C}_{\mathrm{R}} \tag{41}$$

where $\mathrm{d}\mathbf{C}^{-1}/\mathrm{d}\phi_{\mathscr{A}} = [\mathbf{C}_{\mathscr{A}}^{-1} - \mathbf{C}_{\mathscr{B}}^{-1}]$. Since it can be shown that (41) is uniformly positive definite, the Hessian of $\mathscr{F}_{\mathrm{E}}$ (38) is not necessarily positive-definite with the Reuss mixing rule since it represents the difference between two positive-definite matrices both of which vary rather unpredictably throughout the design variable space. One can thus expect that multiple local optima could very well exist as solutions to the optimization problem formulated with the Reuss mixing rule.

The following can thus be stated: Usage of the pure Voigt formulation leads to a uniformly convex strain energy functional $\mathscr{F}_{\mathrm{E}}$, and hence unique solutions of the optimization problem for a fixed mesh discretization of $\boldsymbol{\Omega}_{\mathrm{B}}$, irrespective of the starting point $\mathbf{b}_{\mathrm{o}}$ or the optimization algorithm employed. Usage of the pure Reuss formulation, on the other hand, does not necessarily lead to a uniformly convex functional, and so the solution obtained will depend upon both the starting design $\mathbf{b}_{\mathrm{o}}$ and possibly the optimization algorithm employed. While the unpenalized Voigt solutions to topology optimization problems may be unique, they are generally not very desirable in that they tend to be very grey, containing large regions of mixed materials which can be very difficult to interpret. The pure Reuss solutions, on the other hand, while highly discrete, will generally not be unique. That is, many locally optimal solutions may exist, some of which have performance characteristics approaching those of the global minimum, and some of which do not.

Given the strengths and deficiencies of both extremes, it is desirable to combine the Voigt and Reuss formulations using hybrid mixing rules to obtain the best features of both: the uniqueness of the Voigt solutions, and the interpretability/manufacturability of the Reuss solutions. One way that this has been attempted previously[17, 32] is through continuation methods in which the topology optimization problem is begun with a stiff mixing rule, and gradually transitioned to a penalized formulation. The objective behind the procedure is to get and keep the layout design in the convergence basin of the global optimum while gradually transitioning to a penalized formulation that

will yield a discrete and manufacturable solution. The results shown in Section 6 and those in References 17 and 32 demonstrate that this approach invariably gives, interpretable and manufacturable designs, and the performance (stiffness) of these designs often, but not always, exceeds the performance achieved by beginning with pure Reuss formulations. This behaviour is highly problem dependent and requires further study.

6. DEMONSTRATIVE RESULTS

The challenging examples that follow were chosen to demonstrate the performance of the proposed topology design framework on four published test problems from the literature involving linear elastic structures. In all of the design problems, the optimization solution algorithms employed were variations of a sequential linear programming algorithm SLP with line-searching and an LP subproblem move limit of $\Delta_M = 0 \cdot 05$. SLP methods are proving increasingly popular for large-scale topology optimization applications.[19, 32] Unless otherwise stated, where the structural domains featured gross symmetry, the methods outlined in References 33 and 34 were employed both to enforce symmetry in designs and to reduce the size of the optimization problem.

6.1. The three-load bridge problem

The design domain $\mathbf{\Omega}_D$ shown in Figure 9(a) is originally completely filled with a linear isotropic solid material of properties $\lambda_{solid} = 2{\cdot}69 \times 10^5$ and $\mu_{solid} = 1{\cdot}15 \times 10^5$, and the loading and restraint conditions on the domain are as shown in Figure 7. This is a solid material–void material topology design problem, where the objective is to place the solid material throughout the design domain $\mathbf{\Omega}_D$ to minimize the compliance of the structure for the loading shown, subject to a global volume fraction constraint on the solid phase of 40 per cent. This problem was solved four times with varying Voigt–Reuss mixture parameters and using the filtering method proposed in Section 5, with the default filter parameters.

The pure Voigt solution (Figure 9(a)) is extremely stiff and 'grey', as one might expect due to the incompliant nature of the mixing rule, and thus lacks sharpness and clarity. The authors find that the structural topology solutions obtained with the Voigt mixing rule for a broad range of test problems (beyond those shown here) visually resemble those obtained using stiff rank-2 laminate mixing rules as, for example in References 7 and 9. The material layout designs shown with penalized formulations $\alpha = 0{\cdot}1, 0{\cdot}01, 0{\cdot}0$ in Figures 9(b)–9(d), even when some grey fringes remain, appear for the most part quite interpretable. The designs of Figure 9 should be compared directly with those of Figure 7 to assess the impact of the spatial volume-averaging filters. The topology with local checkerboarding evident in Figure 7 has been largely replaced with material layouts that are virtually checkerboard free in Figure 9. Whereas, the designs in Figure 7(b)–7(d) were virtually discrete, however, the corresponding designs in Figures 9(b)–9(d) show some grey fringes as a result of the filtering process. It is quite likely, that smaller filter parameters (ω_1, ω_2) would eliminate the grey fringes. Alternatively, the designs showing grey fringes can be 'cleaned up' by using a continuation process, in which the optimization is continued with increasingly penalized mixtures. For example, if the fringed design shown in Figure 9(b) is continued with a sequence of hybridization parameters $(\alpha = 0{\cdot}1, 0{\cdot}01, 0{\cdot}0001, 0{\cdot}0)$, the discrete, interpretable design shown in Figure 10(b) is obtained. Although not shown here, the discrete layout designs shown in Figures 9(d) and 10(b) have been tested and found to be stable with mesh refinement.

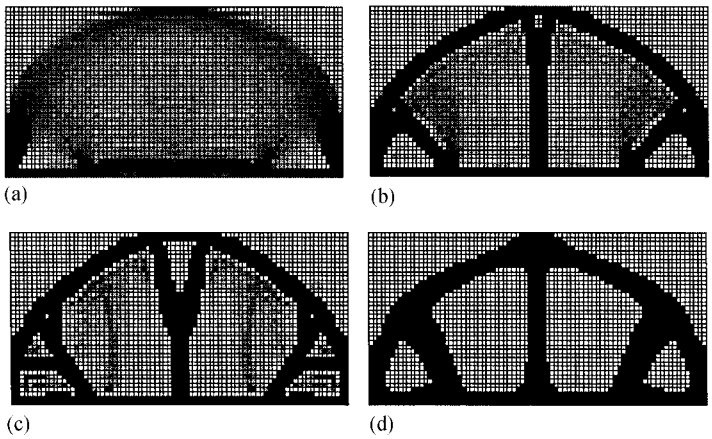

Figure 9. Alternative topology designs and strain energy functional values $\mathscr{F}_E$ for varied mixing rule parameters α: (a) $F_E = 1{\cdot}4121 \times 10^{-2}$, $\alpha = 1{\cdot}0$; (b) $F_E = 2{\cdot}0813 \times 10^{-2}$, $\alpha = 0{\cdot}1$; (c) $F_E = 2{\cdot}3522 \times 10^{-2}$, $\alpha = 0{\cdot}01$; (d) $F_E = 1{\cdot}6933 \times 10^{-2}$, $\alpha = 0{\cdot}00$

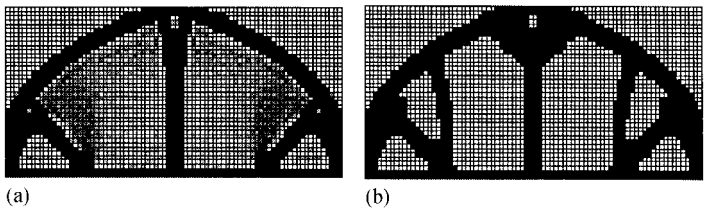

Figure 10. Stable, discrete design (b) obtained from slightly grey design (a) using continuation process with $\alpha = 0{\cdot}01$, $0{\cdot}0001$, $0{\cdot}00$: (a) $F_E = 2{\cdot}0813 \times 10^{-2}$, $\alpha = 0{\cdot}1$; (b) $F_E = 2{\cdot}1858 \times 10^{-2}$, $\alpha = 0{\cdot}0$

6.2. The MBB beam problem

Variations of this challenging test problem involving the design a European Airbus floor beam have been solved previously in References 17, 29 and 35. In the variation of the problem solved here, the simply supported beam features a solid non-designable border $\mathbf{\Omega}_N$ with a designable interior $\mathbf{\Omega}_D$. This problem is solved with $\mathscr{F}_{solid} = \langle \phi_{solid} \rangle - 0{\cdot}50 \leqslant 0$ and with spatial filtering. Figure 11(a) shows a moderately grey layout solution obtained with a hybrid Voigt–Reuss formulation ($\alpha = 0{\cdot}05$) and only moderate filtering. Figure 11(b) shows the layout design that results from a continuation of the same design with a pure Reuss formulation ($\alpha = 0$) and the same filter parameters.

In both the three-load bridge problem and the MBB beam problem, hybrid formulations with filtering have been found to leave fringes of grey mixtures in designs that appear otherwise interpretable. In both problems, when continuation with higher penalization is employed to clean or discretize the grey regions, the structural effect of the grey regions is replaced with the introduction of entirely new structural members and moderate re-design of the existing members as shown in

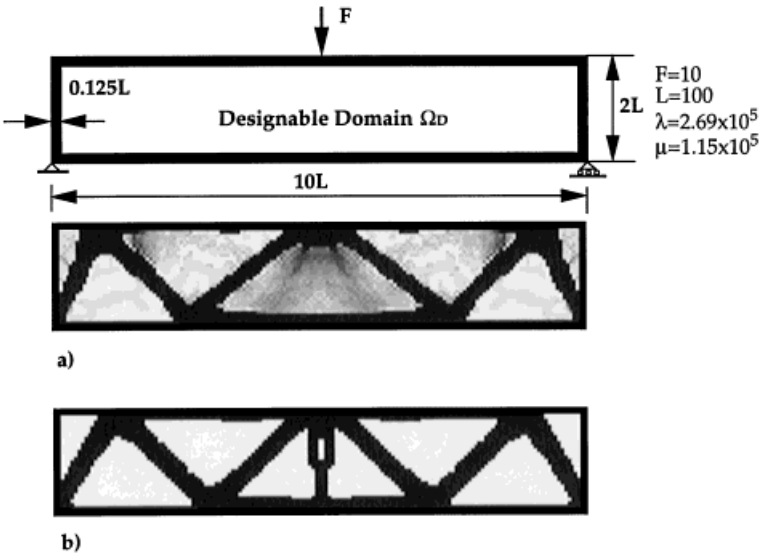

Figure 11. The MBB design problem, and solutions obtained with $\alpha = 0{\cdot}05$ (a), and as a continuation of the same problem with $\alpha = 0{\cdot}0$ (b): (a) $F_E = 1{\cdot}29 \times 10^{-2}$, $\alpha = 0{\cdot}05$, $\omega_1 = 0{\cdot}05$, $\omega_2 = 0{\cdot}025$; (b) $F_E = 1{\cdot}35 \times 10^{-2}$, $\alpha = 0{\cdot}0$, $\omega_1 = 0{\cdot}05$, $\omega_2 = 0{\cdot}025$

Figures 10 and 11. With non-penalized and moderately penalized formulations, the specific effect of residual grey regions can thus be deceptively difficult to interpret.

6.3. The cantilever problem

The cantilever beam design problem (Figure 12) has been used extensively as a test problem by a number of investigators, as for example in References 9, 17, 19, 28, 31 and 36 and with the mis-aligned version of this problem considered to be especially challenging in that it tests the inherent mesh-dependency (if it exists) of alternative topology design formulations. Here, we solve this as a compliance minimization problem with a 25 per cent global solid volume fraction constraint for both an aligned mesh, and a mis-aligned mesh (45×90) consisting of rectangular elements having an aspect ratio of 2:1. All calculations of this problem used filtering with the default filter parameters.

Figure 12(a) shows the pure Reuss solution ($\alpha = 0$) for the aligned mesh problem without symmetry control. Even without symmetry control, the design is symmetric, as one would expect, due to the symmetry of the mesh and the material response to the applied load. Figure 12(b) shows the design obtained when the same basic problem is solved in pure Reuss mode ($\alpha = 0$) with a misaligned mesh of rectangular elements. In this case, there is in fact some mesh dependency of the formulation and a moderately asymmetric design is achieved. Figure 12(c) is a re-solving of the same mis-aligned mesh problem using continuation ($\alpha = 1{\cdot}0$, $0{\cdot}01$, $0{\cdot}0001$, $0{\cdot}0$). The resulting design still shows asymmetry in the design. Finally, to show that symmetric designs can indeed be obtained even when the mesh is asymmetric with respect to the applied loads, the problem is solved once again in pure Reuss mode (Figure 12(d)) with gross symmetry control[33, 34] imposed about the centroidal axis of the beam.

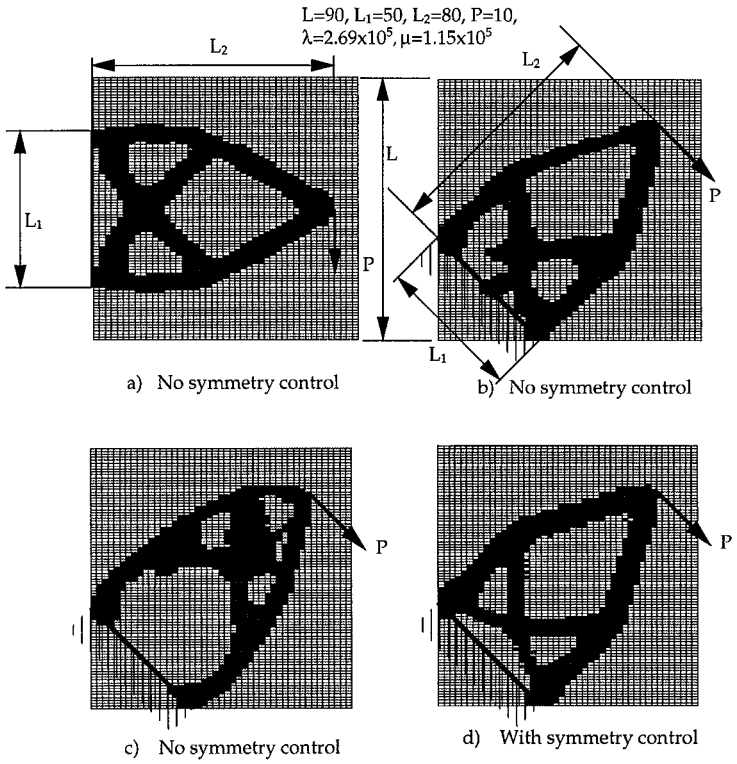

Figure 12. The cantilever design problem and solutions obtained: (a) $F_E = 6{\cdot}96 \times 10^{-3}$, $\alpha = 0{\cdot}0$; (b) $F_E = 8{\cdot}27 \times 10^{-3}$, $\alpha = 0{\cdot}0$; (c) $F_E = 1{\cdot}42 \times 10^{-2}$, $\alpha = 1{\cdot}0$, $0{\cdot}01$, $0{\cdot}0001$, $0{\cdot}0$; (d) $F_E = 7{\cdot}75 \times 10^{-3}$, $\alpha = 0{\cdot}0$

6.4. The trunk lid problem

The trunk lid problem has been previously presented in the research literature.[32, 37] Figure 13(a) shows the full structural domain $\mathbf{\Omega}_B$, the boundary and loading conditions, and the design domain $\mathbf{\Omega}_D$ for the trunk lid problem. Although the boundary and loading conditions are asymmetrical, gross symmetry can easily be imposed on the design via the general methods presented in References 33 and 34. The white region in the structure represents the design domain $\mathbf{\Omega}_D$ and the non-designable black region $\mathbf{\Omega}_N$ contains solid material. A thin shell structure such as the trunk lid uses both bending and membrane action to carry the applied torsional loads. The topology optimization calculations were performed using continuum degenerated shell elements with reduced integration of both transverse shear and membrane stresses to avoid numerical locking phenomena.[38] For the fixed loads shown in Figure 13, the topology design problem was solved to minimize compliance with a global solid volume fraction constraint of 40 per cent in $\mathbf{\Omega}_D$.

The three solutions to this problem presented in Figure 13 were realized with standard filtering but varying hybridization parameters α. The formulations used to achieve the designs shown in Figure 13 are:

(a) $\alpha = 0{\cdot}0$.
(b) $\alpha = 0{\cdot}1$, $0{\cdot}01$, $0{\cdot}001$, $0{\cdot}0$;
(c) $\alpha = 1{\cdot}0$, $0{\cdot}10$, $0{\cdot}01$, $0{\cdot}001$, $0{\cdot}0$.

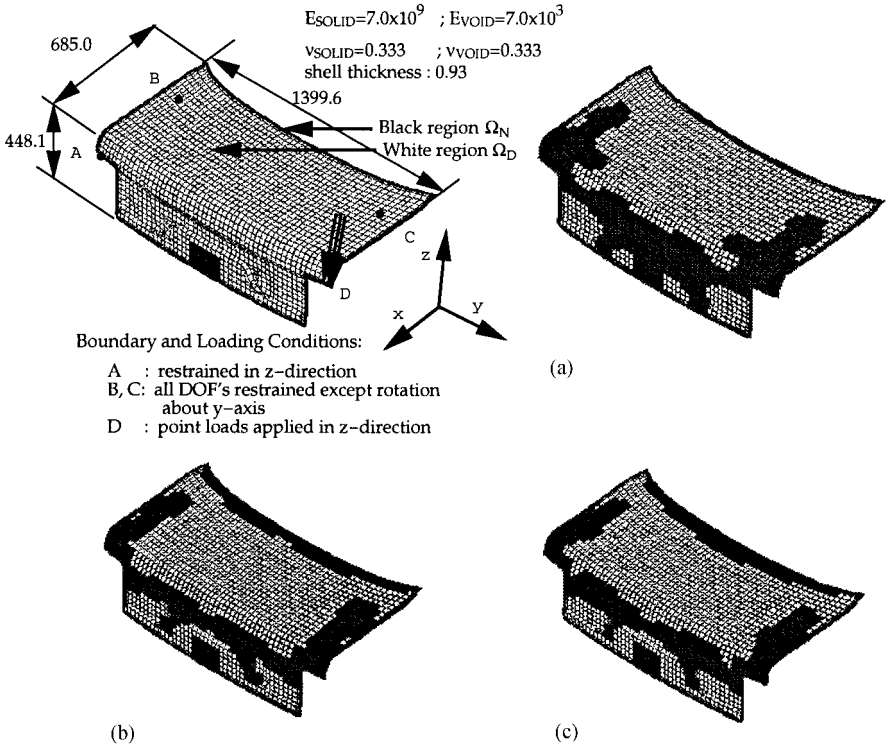

Figure 13. Solutions to the trunk lid problem achieved with alternative formulations: (a) $F_E = 23{\cdot}204$, $\alpha = 0{\cdot}0$; (b) $F_E = 22{\cdot}622$, $\alpha = 0{\cdot}1$, $0{\cdot}01$, $0{\cdot}001$, $0{\cdot}0$; (c) $F_E = 26{\cdot}716$, $\alpha = 1{\cdot}0$, $0{\cdot}1$, $0{\cdot}01$, $0{\cdot}001$, $0{\cdot}0$

All of the solutions presented are clearly stable, interpretable and manufacturable concept designs to carry the specific loads considered. Black regions indicate where structural members should be located to carry the applied loads considered, and white domains represent regions where only minimal skin thickness is required to provide the necessary shielding functions of the trunk lid. The desired effect of continuation strategies discussed in Section 5.2 and employed in the calculations of Figure 13(b) and 13(c) is to obtain unique solutions that approach the performance of the global minimum. Clearly in this case, however, the continuation did not have the desired result, since the designs of Figure 13(b) and 13(c) are noticeably different, and their performance characteristics are roughly equivalent to that of the pure Reuss design Figure 13(a). It is thus apparent that further work to implement criterion based, and yet efficient, continuation methods is required. In the interim, however, it is evident that the proposed formulation yields a number of competing, locally optimum designs that are highly discrete, stable, and interpretable.

7. SUMMARY AND CONCLUSIONS

A continuous, variable-topology material layout formulation using mixtures characterized simply by volume fractions has been implemented and tested on a set of four representative structural topology test problems from the literature. The constitutive behaviour of the mixtures is

described by the classical Voigt and Reuss mixing rules and hybrid combinations thereof. Due to the bounding properties of the Voigt and Reuss mixing rules, the proposed hybrid formulation essentially encompasses all others: With $\alpha = 1$ the maximal stiffness pure Voigt formulation is achieved; with $\alpha = 0$ the maximal compliance pure Reuss formulation is achieved. The strengths and weaknesses of both extremes have been noted, and the hybrid formulation has been employed here in assorted attempts to obtain the advantages of both extremes: the uniqueness and high performance of the Voigt solutions and the discreteness and interpretability of the Reuss solutions. This was attempted with *ad hoc* selection of α in continuation procedures based on heuristic reasoning. In future efforts, control of α during the optimization process will be investigated by maintaining positive definiteness of the Hessian (38).

A careful inspection of the results obtained on the four-test problems treated in Section 6 would perhaps lead some to conclude that with the proposed concept design formulation it is generally best to resort directly to the Reuss formulation. This appears worth trying for most problems, since there are cases (i.e. the three-load bridge problem; the trunk lid problem; the cantilever problem; and numerous others) where the best discrete continuum solutions are in fact obtained (most efficiently) by resorting directly to the pure Reuss formulation. There are counterexamples, however (the MBB beam problem, in particular) where resorting directly to the pure Reuss formulation ($\alpha = 0$) can yield low-performance design solutions. This behaviour is highly problem dependent and warrants further study both in terms of formulation of the design problem, and in terms of optimization solution methods. With the proposed design methods each new problem being solved should generally be attempted (in addition to the pure Reuss formulation) with continuation methods as well, in which case one begins with the Voigt formulation and gradually transitions to the Reuss formulation. Given a number of competing designs achieved with various continuation strategies, a specific design can be chosen for further refinement in the detailed design stage.

The proposed Voigt–Reuss formulation studied here was originally conceived by the authors[30] for the variable topology layout design of multiple solid phases in the unit cells of periodic composites. Perceived benefits of the Voigt–Reuss formulation for such composite design applications are that it can be used to combine multiple general solid materials with linear elastic and/or more general behaviours. In this paper, the formulation was applied exclusively to structural topology applications involving a linear elastic solid phase and a void phase. The performance of the proposed formulation on this class of problems is encouraging. A key ingredient of obtaining the stable and interpretable solutions presented herein with low-order finite element methods was the usage of spatial filtering of the design variables as discussed in Section 5.1. The mesh-based filtering procedure employed is certainly not unique, but it can be used with a wide range of elements and clearly solves the problem of checkerboarding instabilities and leads to material layout designs that are stable with mesh refinement.

REFERENCES

1. W. Gutkowski, J. Bauer and Z. Iwanow, 'Discrete structural optimization', *Comput. Methods Appl. Mech. Eng.*, **51,** 71–78 (1985).
2. S. D. Rajan, 'Sizing, shape and topology design optimization of trusses using genetic algorithm', *J. Struct. Eng.*, **1110,** 1480–1487 (1995).
3. R. V. Kohn and G. Strang, 'Optimal design and relaxation of variational problems', *Commun. Pure Appl. Math.*, **39** Part I 113–137; Part II 139–182; Part III 353–377 (1986).
4. M. P. Bendsoe and N. Kikuchi, 'Generating optimal topology in structural design using a homogenization method', *Comput. Methods Appl. Mech. Eng.*, **71,** 197–224 (1988).
5. C. C. Swan and J. S. Arora, 'Topology design of material layout in structured composites of high stiffness and strength', *Struct. Optim.*, (1997) in press.

6. C. C. Swan and I. Kosaka, 'Voigt–Reuss topology optimization for structures with inelastic material behaviors', (1997), to appear in *Int. J. Numer. Meth. Engng.*
7. C. S. Jog, R. B. Haber and M. P. Bendsoe, 'Topology design with optimized, self-adaptive materials', *Int. J. Numer. Meth. Engng.*, **37,** 1323–1350 (1994).
8. M. P. Bendsoe, A. R. Diaz, R. Lipton and J. E. Taylor, 'Optimal design of material properties and material distribution for multiple loading conditions', *Int. J. Numer. Meth. Engng.*, **38,** 1149–1170 (1995).
9. G. Allaire and R. V. Kohn, 'Topology optimal design and optimal shape design using homogenization', in: M. P. Bendsoe and C. A. Mota Soares (eds.), Topology Design of Structures, Kluwer Academic Publishers, Dordrecht/Boston, 1993, pp. 207–218.
10. P. Pedersen, 'Bounds on elastic energy in solids of orthotropic materials', *Struct. Optim.*, **2,** 55–63 (1990).
11. H. C. Gea and Y. Fu, '3-D shell topology optimization using a design domain method', *SAE preprint 951105*, 1995, pp. 245–251.
12. T. Mori and K. Tanaka, 'Average stress in matrix and average elastic energy of materials with misfitting inclusions', *ACTA Metall.*, **21,** 571–574 (1973).
13. J. Eshelby, 'The determination of the elastic field of an ellipsoidal inclusion and related problems', *Proc. Roy. Soc. London*, **A241,** 379–396 (1957).
14. J. W. Ju and T. M. Chen, 'Micromechanics and effective elastoplastic behaviour of two-phase metal matrix composites', *J. Eng. Mater. Technol. Trans. ASME*, **116,** 310–318 (1994).
15. M. P. Bendsoe, 'Optimal shape design as a material distribution problem', *Struct. Optim.*, **1,** 193–202 (1989).
16. E. Ramm, K.-U. Bletzinger, R. Reitinger and K. Maute, 'The challenge of structural optimization', in B. H. V. Topping and M. Papadrakakis (eds.), Advances in Structural Optimization, Civil-Comp Press, Edinburgh, UK, 1994, pp. 27–53.
17. O. Sigmund, 'Design of material structures using topology optimization', *Report S69*, Danish Center for Applied Mathematics and Mechanics, Technical University of Denmark, Lyngby, Denmark, 1994.
18. H. P. Mlejnek and R. Schirrmacher, 'An engineer's approach to optimal material distribution and shape finding', *Comput. Methods Appl. Mech. Eng.*, **106,** 1–26 (1993).
19. R. J. Yang and C. H. Chuang, 'Optimal topology design using linear programming', *Comput. Struct.*, **52,** 265–275 (1994).
20. A. Reuss, *Z. Angew. Math. Mech.*, **9** (1929).
21. W. Voigt, *Wied Ann.*, **38** (1889).
22. J. Aboudi, *Mechanics of Composite Materials*: *A Unified Micromechanical Approach*, Elsevier, Amsterdam, 1991.
23. C. S. Jog and R. B. Haber, 'Stability of finite element models for distributed-parameter optimization and topology design', *Comput. Methods Appl. Mech. Eng.*, **130,** 203–226 (1996).
24. S. C. Cowin, 'Bone stress adaptation models', *J. Biomech. Eng.*, **115,** 528–533 (1993).
25. H. Weinans, R. Huiskes and H. J. Grootenboer, 'The behaviour of adaptive bone-remodelling simulation models', *J. Biomech.*, **25,** 1425–1441 (1992).
26. A. Diaz and O. Sigmund, 'Checkerboard patterns in layout optimization', *Struct. Optim.*, **10,** 40–45 (1995).
27. M. G. Mullender, R. Huiskes and H. Weinans, 'A physiological approach to the simulation of bone remodelling as a self-organizational control process', *J. Biomech.*, **27,** 1389–1394 (1994).
28. M. P. Bendsoe, A. Diaz and N. Kikuchi, 'Topology and generalized layout optimization of elastic structures', in M. P. Bendsoe and C. A. Mota Soares (eds.), *Topology Design of Structures*, Kluwer Academic Publishers, Dordrecht/Boston, 1993, pp. 159–205.
29. R. B. Haber, C. S. Jog and M. P. Bendsoe, 'A new approach to variable-topology shape design using a constraint on perimeter', *Struct. Optim.*, **11,** 1–12 (1996).
30. C. C. Swan and I. Kosaka, 'Homogenization-based analysis and design of composites', *Comput. Struct.*, (1997), in press.
31. A. R. Diaz and M. P. Bendsoe, 'Shape optimization of structures for multiple loading conditions using a homogenization method', *Struct. Optim.*, **4,** 17–22 (1992).
32. C. C. Swan, J. S. Arora, I. Kosaka and M. W. Huang, 'Structural topology design of civil structures using SLP and classical mixing rules', (1996), pending.
33. C. C. Swan and I. Kosaka, 'Symmetry control in variable topology shape design', in M. Rysz, L. A. Godoy, L. E. Suarez (eds.), *Applied Mechanics in the Americas*, **5,** 381–384 (1997).
34. C. C. Swan and I. Kosaka, 'Topology optimization for discrete, symmetric and stable material layout optimization', in B. H. V. Topping (ed.), *Advances in Optimization for Structural Engineering*, Civil-Comp., Edinburgh, 1996.
35. J. Rasmussen, J. Thomsen and N. Olhoff, 'Integrating topology and boundary variation design methods in a CAD system', in M. P. Bendsoe and C. A. Mota Soares (eds.), *Topology Design of Structures*, Kluwer Academic Publishers, Dordrecht/Boston, 1993, pp. 483–499.
36. K. Suzuki and N. Kikuchi, 'A homogenization method for shape and topology optimization', *Comput. Methods Appl. Mech. Eng.*, **93,** 291–318 (1991).
37. M. Chirehdast, S. Sankaranarayanan, S. D. Ambo and R. P. Johanson, 'Validation of topology optimization for component design', *SDM Preprint*, 1994.
38. T. J. R. Hughes, *The Finite Element Method*, Prentice-Hall, Englewood Cliffs, N.J., 1987.

